electronics

MDPI

Article

Nested Kriging with Variable Domain Thickness for Rapid Surrogate Modeling and Design Optimization of Antennas

Anna Pietrenko-Dabrowska [1,*] and Slawomir Koziel [1,2]

[1] Faculty of Electronics, Telecommunications and Informatics, Gdansk University of Technology, 80-233 Gdansk, Poland; koziel@ru.is

[2] Engineering Optimization & Modeling Center, Reykjavik University, 101 Reykjavik, Iceland

* Correspondence: anna.dabrowska@pg.edu.pl

Received: 2 September 2020; Accepted: 30 September 2020; Published: 2 October 2020



Abstract: Design of modern antennas faces numerous difficulties, partially rooted in stringent specifications imposed on both electrical and field characteristics, demands concerning various functionalities (circular polarization, pattern diversity, band-notch operation), but also constraints imposed upon the physical size of the radiators. Conducting the design process at the level of full-wave electromagnetic (EM) simulations, otherwise dictated by reliability, entails considerable computational expenses, which is another and a serious challenge. It is especially pronounced for the procedures involving repetitive EM analyses, e.g., parametric optimization. Utilization of fast surrogate models as a way of mitigating this issue has been fostered in the recent literature. Unfortunately, construction of reliable surrogates for antenna structures is hindered by their highly nonlinear responses and even more by the utility requirements: design-ready models are to be valid over wide ranges of operating conditions and geometry parameters. Recently proposed performance-driven modeling, especially the nested kriging framework, addresses these difficulties by confining the surrogate model domain to a region that encapsulates the designs being optimum with respect to the relevant figures of interest. The result is a dramatic reduction of the number of training samples needed to render a usable model. This paper introduces a variable-thickness domain, which is an important advancement over the basic nested kriging. The major benefit demonstrated using two antenna examples is a further and significant (up to seventy percent) reduction of the training data acquisition cost. It is achieved while ensuring that the model domain covers the regions containing optimum designs for various sets of performance specifications.

Keywords: antenna modeling; surrogate modeling; nested kriging; domain confinement; variable-thickness domain; simulation-driven design

1. Introduction

Contemporary antenna structures are designed to meet the demands pertaining to different application areas, including wireless communications [1] (along with the emerging 5G technology [2,3]), satellite communications [4], medical imaging [5], or internet of things (IoT) [6]. In many cases, various functionalities have to be implemented including multi-band operation [7], circular polarization [8], band notches [9], MIMO operation [10], or pattern diversity [11]. At the same time, reduction of the physical size of radiators is of concern for a growing number of situations (e.g., wearable [12] and implantable devices [13]). In pursuit of fulfilling the stringent specifications, increasingly complex antenna topologies are being developed. Their evaluation requires full-wave electromagnetic (EM) analysis because other means are either unavailable or (as equivalent network models) can only be

used for yielding rough initial designs that need further tuning [14]. Nowadays, EM-driven design is ubiquitous, but its downside is high computational cost. This becomes a practical issue whenever multiple simulations are necessary. A typical task is parameter adjustment [15,16]. It is imperative for most antenna structures but generates considerable CPU expenditures, particularly when reasonable initial design is not available, or the global search needs to be involved [17].

Expediting design optimization can be realized at the algorithmic level. Representative examples are the gradient-based procedures where the speedup can be achieved by lowering the cost of antenna response Jacobian estimation using adjoint sensitivities [18,19], or by suppressing finite-differentiation sensitivity updates based on various criteria, e.g., monitoring design relocation [20] or gradient changes between the algorithm iterations [21]. The employment of fast surrogate models provides viable alternatives. These can be realized in the context of local [22] or global optimization [23]. For the former, the surrogates are typically constructed along the optimization path, and can be data-driven (polynomial regression [24], kriging [25], neural networks [26], polynomial chaos expansion [27]) or physics-based (space mapping [28,29], response correction [30], feature-based optimization [31]), normally obtained from underlying low-fidelity models (in the case of antennas most often being coarse-mesh EM simulations [32]). Global surrogate-assisted optimization often involves machine learning techniques [33] but also all kinds of approximation surrogates [34]. In this context, sequential sampling methods are typically employed [35], where iterative allocation of the infill points can be aimed at improving the predictive power of the model, searching for the global optimum or the combination thereof [36].

Utilization of the stand-alone surrogate models as replacements of CPU-heavy EM simulations has been fostered in the literature as a way of accelerating various simulation-driven design procedures, including design closure [37–39]. Data-driven surrogates seem to be especially attractive for these purposes due to their versatility and widespread availability (e.g., [40,41]). Well established and popular approximation techniques include polynomial regression [36], artificial neural networks [42], radial basis functions (RBF) [37], kriging interpolation [36], Gaussian process regression (GPR) [38], or support vector regression (SVR) [43]. Unfortunately, conventional methods are severely limited when applied to antenna problems. The primary challenges include nonlinearity of antenna characteristics, the curse of dimensionality affecting the modeling process due to a typically large number of geometry/material parameters that need to be handled, as well as the need for covering wide ranges of operating conditions and designable parameters. The latter is critical from the point of view of practical usefulness of the surrogate for design purposes. Alleviating these difficulties is possible in specific situations using the methods such as high-dimensional model representation (HDMR) [44], least-angle regression [45], or incorporation of variable-fidelity models (two-stage GPR [46], co-kriging [47], Bayesian model fusion [48]).

Model domain confinement has been recently suggested as an alternative approach to computationally efficient surrogate modeling [49–51]. By focusing the modeling process on the region containing designs that are optimum with respect to the selected performance figures (e.g., operating frequencies of a multi-band antenna) or material parameters (e.g., relative permittivity of the dielectric substrate the antenna is implemented on), reliable surrogate can be rendered over wide ranges of operating conditions using small training data sets. Identification of such regions is realized with the help of pre-existing reference designs [50], which could be available from the previous design work with the same structure or obtained as a part of the modeling procedure.

One of the most recent methods adopting the domain confinement approach is the nested kriging framework [51]. The two kriging metamodels are utilized: the first-level one to establish the region of interest (model domain), and the second-level model being the actual surrogate. The important advantage of the technique is a straightforward arrangement of uniform training data sampling as well as model optimization, both enabled by a one-to-one mapping between the unity interval and the surrogate domain being a part of the formulation of the procedure [51]. The critical (scalar) control parameter of nested kriging is the thickness coefficient determining the ratio between the lateral

and tangential size of the domain. Its value establishes the trade-off between the model predictive power and the coverage of the regions containing potentially optimum antenna designs for various sets of performance specifications. This paper proposes a variable-thickness domain for nested kriging, where the thickness parameter is a function of the objective space vectors. The keystones of the approach are the reference design triangulation and an appropriate mapping defined over the expansion coefficients of the objective vector with respect to the vertices of the simplexes being a result of the triangulation process. Using this mapping, the domain thickness is maintained small in the vicinity of the reference designs (which are optimal by definition) and increases towards the simplex centers (where the first-level model deviates the most from the optimum design manifold). The variable-thickness domain method permits the construction of reliable surrogates using significantly (by up to seventy percent) smaller data sets than required by the fixed thickness version. The computational benefits are achieved without compromising the model coverage in terms of geometry parameter and operating condition ranges. These properties are validated using two antenna examples as well as benchmarking against conventional modeling methods (kriging, RBF) and the original nested kriging. The major novelties and technical contributions of the paper, beyond what has been presented in the literature so far, include: (i) introduction of the concept of variable-thickness domain including its rigorous analytical formulation, (ii) incorporation of the concept into the nested kriging modeling framework, (iii) demonstration of significant computational benefits that can be obtained (up to seventy percent savings in terms of the training data acquisition cost) as compared to the state-of-the-art approaches, without compromising the model predictive power, (iv) demonstration of the model efficacy as antenna design tool. To the best of authors' knowledge, the presented approach is the first modeling framework that permits construction of fast and reliable surrogates of antenna structures within broad ranges of geometry and operating parameters while using such a small number of data samples.

2. Surrogate Modeling by Nested Kriging

For the purpose of self-containment, this section briefly recalls the formulation of the nested kriging modeling framework. The variable-thickness domain concept is outlined in Section 3, whereas its numerical validation can be found in Section 4.

2.1. First-Level Surrogate

The nested kriging framework takes advantage of the correlations between antenna geometry parameters corresponding to the designs that are optimum with respect to the typical figures of interest [49]. For example, antenna re-design for various operating frequencies normally entails synchronized adjustment of the parameters. The parameter sets being away from these correlation patterns are of poor quality and excluding them from the modelling process may be beneficial from the point of view of the computational efficiency. This is in opposition to conventional domains determined by the lower and upper bounds for design parameters, which are indiscriminative with respect to the aforementioned correlations. In nested kriging, identification of the regions containing high-quality designs is realized using a set of reference designs and the first-level surrogate as elaborated on below.

We denote by $\boldsymbol{x} = [x_1 \ \ldots \ x_n]^T$ the vector of antenna parameters. The (conventional) parameter space X is defined by the lower and upper bounds $\boldsymbol{l} = [l_1 \ \ldots \ , \ l_n]^T$ and $\boldsymbol{u} = [u_1 \ \ldots \ , \ u_n]^T$, so that $l_k \leq x_k \leq u_k$ for $k = 1, \ldots , n$. Furthermore, we denote by f_k, $k = 1, \ldots , N$, the figures of interest pertinent to the design task at hand, operating conditions, or material parameters (e.g., operating frequency, bandwidth, or substrate permittivity assuming that the antenna is to be re-designed for various substrates). The ranges $f_{k.\min} \leq f_k^{(j)} \leq f_{k.\max}$, $k = 1, \ldots , N$, define the objective space F, i.e., the region over which the surrogate model is to be valid.

The design optimality is understood, for a given objective vector $\boldsymbol{f} \in F$, in the sense of minimizing the functional $U(\boldsymbol{x},\boldsymbol{f})$, where U is the scalar merit function which quantifies the design quality. In other words, the optimum design $\boldsymbol{x}^*$ is given as

$$\boldsymbol{x}^* = U_F(\boldsymbol{f}) = \underset{\boldsymbol{x}}{\operatorname{argmin}} U(\boldsymbol{x},\boldsymbol{f}) \tag{1}$$

We also define

$$U_F(F) = \{U_F(\boldsymbol{f}) : \boldsymbol{f} \in F\} \tag{2}$$

which is the manifold consisting the designs being optimum in the sense of (1) for all $\boldsymbol{f} \in F$.

For the sake of computational efficiency, it is advantageous to construct the surrogate model in the vicinity of $U_F(F)$. Within the nested kriging framework, the first approximation of this set is obtained using the reference designs $\boldsymbol{x}^{(j)} = [x_1{}^{(j)} \ \dots \ x_n{}^{(j)}]^T$ $j = 1, \dots, p$, optimized with respect to the objective vectors $\boldsymbol{f}^{(j)} = [f_1{}^{(j)} \ \dots \ f_N{}^{(j)}]$; $\boldsymbol{f}^{(j)}$ should be allocated in a possibly uniform manner in F. As mentioned before, $\boldsymbol{x}^{(j)}$ may be available from the previous design work on the same structure or obtained specifically for the purpose of surrogate model construction.

The first-level surrogate $\boldsymbol{s}_I(\boldsymbol{f})$: $F \rightarrow X$ is identified as a kriging interpolation model [51] using $\{\boldsymbol{f}^{(j)},\boldsymbol{x}^{(j)}\}$, $j = 1, \dots, p$, as the training set. Figure 1 shows a graphical illustration of these concepts. Note that $\boldsymbol{s}_I(F)$ (the image of F) approximates $U_F(F)$ but it does not coincide with it because the number of the reference designs is normally limited. It should be noted that the geometry of the reference set in the objective space is generally different than that in the parameter space; however, the reference points in the parameter space are arranged along the manifold $U_F(F)$, i.e., the object of the same dimensionality as F.

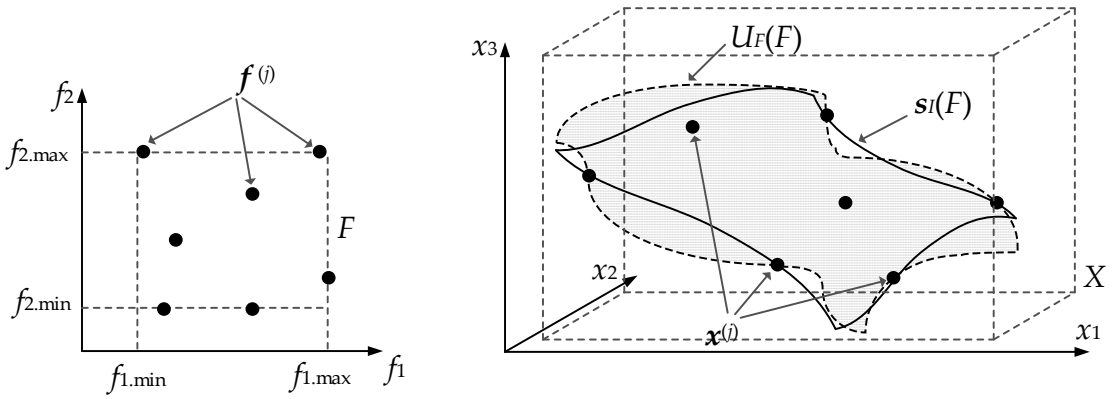


Figure 1. Fundamentals of the nested kriging concept (here, shown for two performance figures and three-dimensional parameter space): (**a**) objective space F, (**b**) parameter space X, the reference designs, the optimum design manifold $U_F(F)$, and the first-level model image $\boldsymbol{s}_I(F)$. The manifolds $U_F(F)$ and $\boldsymbol{s}_I(F)$ do not coincide for all $\boldsymbol{f} \in F$ but the agreement is perfect for all reference designs $\boldsymbol{x}^{(j)}$, which are optimal in the sense of (1).

2.2. Domain Definition

Due to imperfect approximation of $U_F(F)$ by $\boldsymbol{s}_I(F)$ it is necessary to extend the latter so that all (or most) of the designs $U_F(\boldsymbol{f})$ are included. In [51], the extension is implemented using the vectors normal to $\boldsymbol{s}_I(F)$. We denote by $\{\boldsymbol{v}_n{}^{(k)}(\boldsymbol{f})\}$, $k = 1, \dots, n - N$, an orthonormal basis of vectors normal to $\boldsymbol{s}_I(F)$ at $\boldsymbol{f}$.

Additional notation is also used: $\boldsymbol{x}_{\max} = \max\{\boldsymbol{x}^{(k)}, k = 1, \ldots, p\}$, $\boldsymbol{x}_{\min} = \min\{\boldsymbol{x}^{(k)}, k = 1, \ldots, p\}$, and $\boldsymbol{x}_d = \boldsymbol{x}_{\max} - \boldsymbol{x}_{\min}$, which quantifies the parameter variations within $\boldsymbol{s}_I(F)$. The extension coefficients are then defined as

$$\boldsymbol{\alpha}(\boldsymbol{f}) = [\alpha_1(\boldsymbol{f}) \ \ldots \ \alpha_{n-N}(\boldsymbol{f})]^T = 0.5T\left[|\boldsymbol{x}_d \boldsymbol{v}_n^{(1)}(\boldsymbol{f})| \ \ldots \ |\boldsymbol{x}_d \boldsymbol{v}_n^{(n-N)}(\boldsymbol{f})|\right]^T \tag{3}$$

where T is a user-defined thickness parameter. The surrogate model domain X_S is allocated between the manifolds M_+ and M_-

$$M_\pm = \left\{\boldsymbol{x} \in X : \boldsymbol{x} = \boldsymbol{s}_I(\boldsymbol{f}) \pm \sum\nolimits_{k=1}^{n-N} \alpha_k(\boldsymbol{f}) \boldsymbol{v}_n^{(k)}(\boldsymbol{f})\right\} \tag{4}$$

We have

$$X_S = \left\{ \begin{array}{c} \boldsymbol{x} = \boldsymbol{s}_I(\boldsymbol{f}) + \sum\limits_{k=1}^{n-N} \lambda_k \alpha_k(\boldsymbol{f}) \boldsymbol{v}_n^{(k)}(\boldsymbol{f}) : \boldsymbol{f} \in F, \\ -1 \le \lambda_k \le 1, \, k = 1, \ldots, n-N \end{array} \right\} \tag{5}$$

A graphical illustration of the manifolds M_+, M_-, and the domain X_S has been provided in Figure 2. The second-level (i.e., the actual) surrogate is implemented as a kriging interpolation model over the domain X_S. The training data is $\{\boldsymbol{x}_B^{(k)}, \boldsymbol{R}(\boldsymbol{x}_B^{(k)})\}_{k = 1, \ldots, NB}$, where $\boldsymbol{x}_B^{(k)} \in X_S$ are uniformly allocated samples, whereas $\boldsymbol{R}$ stands for the response of the EM-simulation model of the antenna. Detailed information about the design of experiments (sampling) procedure can be found in [51] (see also Section 3.3).

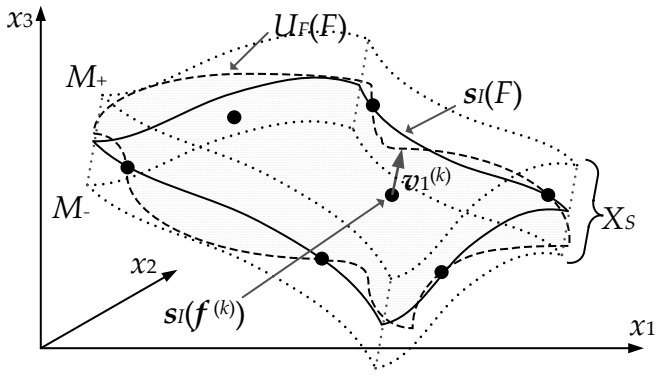


Figure 2. The image $\boldsymbol{s}_I(F)$ of the first-level surrogate model and the normal vector $\boldsymbol{v}_1{}^{(k)}$ at $\boldsymbol{f}^{(k)}$; the manifolds M_- and M_+ and the surrogate model domain X_S defined as the orthogonal extension of $\boldsymbol{s}_I(F)$.

As demonstrated in [51], confining the surrogate model domain to X_S, the volume of which is significantly smaller than the volume of X, brings in considerable computational benefits. The major advantage is a possibility of constructing reliable surrogates using a small number of training samples and without formally restricting the ranges of antenna parameters and operating conditions the model is valid for. Even more importantly, these benefits are especially pronounced in higher-dimensional spaces where modeling within the conventional domain X is often computationally prohibitive.

3. Variable-Thickness Domain

This section discusses the importance of the surrogate model thickness parameter T in the light of the trade-offs between the model predictive power, the cost of training data acquisition, as well as the model utility in the sense of the domain encapsulating the optimum design manifold $U_F(F)$. The concept and implementation of variable-thickness domain is subsequently introduced along with its incorporation into the nested kriging modelling framework.

3.1. Domain Thickness: Model Accuracy vs. Utility Trade-Offs

The thickness parameter T plays an essential role in the nested kriging framework. On one hand, it determines the volume of the domain X_S. Increasing the value of T by a factor of two enlarges the domain by a factor 2^{n-N}, which may be orders of magnitude for highly-dimensional space. This directly affects the number of training data samples required to yield the accurate model. In particular, keeping T at low values is beneficial for computational efficiency. On the other hand, reducing the domain thickness leads to keeping a part (or even a majority) of the optimum design manifold $U_F(F)$ out of X_S. This compromises the design utility of the surrogate because the true antenna optimum becomes unattainable for certain regions of the objective space as indicated in Figure 3. Thus, the trade-off is to set T at the minimum value ensuring that most of $U_F(F)$ is in X_S. Clearly, this leaves a very limited room for reducing the cost of training data acquisition given a target level of the model error.

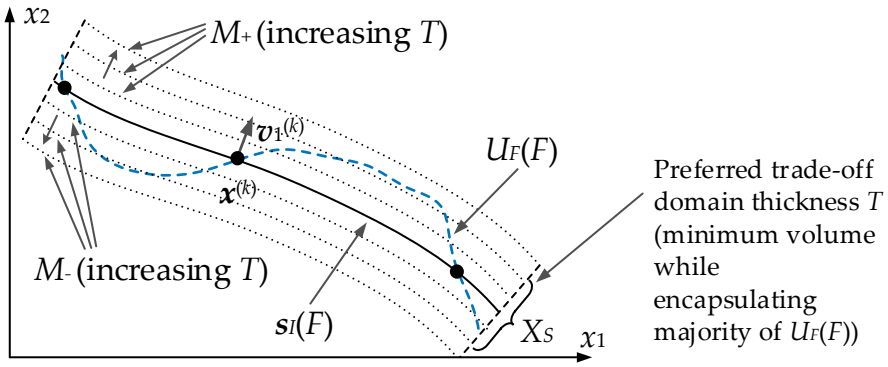


Figure 3. The meaning of the domain thickness parameter T, here, explained for two-dimensional parameter space. Increasing T enlarges the model domain which allows for encapsulating the optimum design manifold $U_F(F)$. At the same time, larger domain requires more training samples to render reliable surrogate. The desired trade-off is to find the minimum value of T enabling incorporation of the majority of $U_F(F)$ into X_S.

3.2. Variable-Thickness Domain

The surrogate model domain defined using an appropriate value of the thickness parameter T (cf. Figure 3) ensures incorporation of the majority of the optimum design manifold $U_F(F)$. At the same time, maintaining fixed T for the entire objective space is not really a necessity.

In particular, as $U_F(F)$ coincides with $\boldsymbol{s}_I(F)$ (the image of F through the first-level surrogate) at all reference designs $\boldsymbol{x}^{(j)}$, at these points, the required domain thickness is zero. Based on these observations, this section introduces a variable thickness domain as a mean to reduce the number of training data samples without compromising the model predictive power. The prerequisites are as follows:

The thickness parameter should be a function of the objective vector $\boldsymbol{f}$, i.e., $T = T(\boldsymbol{f})$;

$T(\boldsymbol{f}^{(j)}) = 0$ for all $j = 1, \ldots, p$, i.e., the domain thickness is zero for all reference designs $\boldsymbol{x}^{(j)} = \boldsymbol{s}_I(\boldsymbol{f}^{(j)})$;

$T(\boldsymbol{f}) = T_{\max}$ (the T-value ensuring $U_F(F) \subset X_S$) for $\boldsymbol{f}$ corresponding to objective space locations where the expected first-level surrogate inaccuracy (w.r.t. $U_F(F)$) is the highest;

$T(\boldsymbol{f})$ changes monotonically for intermediate locations.

The first task is to determine vectors $\boldsymbol{f}$ for which $\|\boldsymbol{s}_I(\boldsymbol{f}) - U_F(\boldsymbol{f})\|$ is maximized. One option would be to identify locations maximizing the mean square error (MSE) of the first-level model, which can be determined directly from the formulation of the kriging interpolation surrogate [52]. Another approach is to make a reasonable assumption that the error is the highest near the geometrical centers of the simplexes $S^{(j)}$, $j = 1, \ldots, N_S$, obtained by triangulating the reference designs, cf. Figure 4. Here, Delaunay triangulation is employed [53] to avoid degenerated simplexes. The simplex centers in the objective space will be denoted as $\boldsymbol{f}_T{}^{(j)}$; their parameter space counterparts are $\boldsymbol{x}_T{}^{(j)} = \boldsymbol{s}_I(\boldsymbol{f}^{(j)})$.

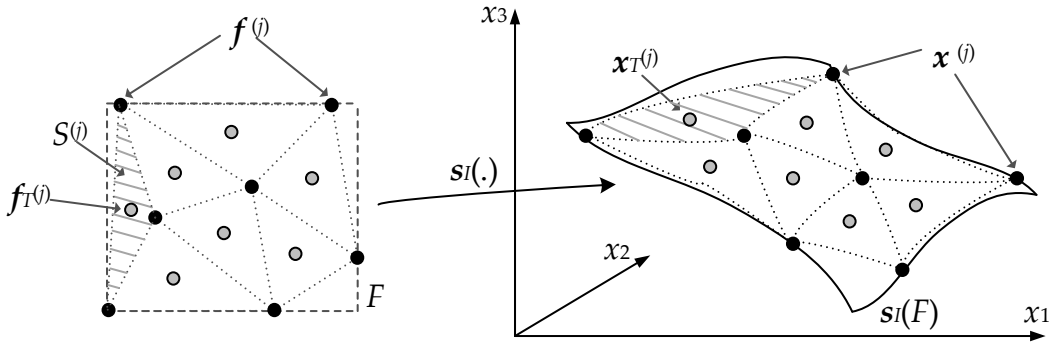


Figure 4. Triangulation of the reference designs performed in the objective space. The centers $\boldsymbol{f}_T^{(j)}$ of the resulting simplexes $S^{(j)}$ are mapped into the parameter space as $\boldsymbol{x}_T^{(j)} = \boldsymbol{s}_I(\boldsymbol{f}_T^{(j)})$.

In order to develop the analytical form of the thickness function $T(\boldsymbol{f})$, the location of any $\boldsymbol{f} \in F$ with respect to the simplexes $S^{(j)}$ has to be established. Let $\boldsymbol{x}^{(j.k)}$, $k = 1, \ldots, N+1$, be the simplex vertices, where $\boldsymbol{x}^{(j.k)} \in \{\boldsymbol{x}^{(1)}, \ldots, \boldsymbol{x}^{(p)}\}$ (the set of reference designs) for $j = 1, \ldots, N_S$, and $k = 1, \ldots, N+1$. For any $j = 1, \ldots, N_S$, the following expansion holds

$$\boldsymbol{f} = \sum_{k=1}^{N+1} a_{j.k}(\boldsymbol{f})\boldsymbol{x}^{(j.k)} \tag{6}$$

where $a_{j.1}(\boldsymbol{f}) + \ldots + a_{j.N+1}(\boldsymbol{f}) = 1$. Let $J(\boldsymbol{f})$ be any j for which $\min\{k{:}a_{j.k}(\boldsymbol{f}) \geq 0\}$. It follows that $\boldsymbol{f} \in H_{conv}(S^{(J(\boldsymbol{f}))})$, where $H_{conv}(S)$ is the convex hull of S. Note that $a_{j.k}(\boldsymbol{f}_T^{(i)}) = (N+1)^{-1}$ for $j = J(\boldsymbol{f}_T^{(i)})$ and all $i = 1, \ldots, N_S$ (recall that $\boldsymbol{f}_T^{(i)}$ were the simplex centers). At the same time, $a_{j.k}(\boldsymbol{f}^{(i)}) = 1$ for a certain $k = 1, \ldots, N+1$, and zero for the remaining values of k. Furthermore, for $N > 1$, the expansion coefficients assume "intermediate" distributions for $\boldsymbol{f}$ being at the boundaries between the simplexes. For example, if $N = 2$, then, for $\boldsymbol{f}$ allocated at the center of the edge between two adjacent simplexes, we have $a_{j.k} = 1/N$ for two out of three values of k and zero for the remaining one. These examples indicate that it is reasonable to decide upon the analytical form of the $T(\boldsymbol{f})$ function based on the standard distribution $std([a_{j.1} \ldots a_{j.N+1}])$ of the expansion coefficients $a_{j.k}$. In particular, this distribution is zero for the simplex centers and attains its maximum equal to $std(E_{N+1})$, where the $(N+1) \times 1$ vector $E_{N+1} = [1\ 0 \ldots 0]^T$, for all reference designs.

This prompts us to the following definition

$$T(\boldsymbol{f}) = T_{\max}\left[1 - std\left([a_{J(\boldsymbol{f}).1} \ldots a_{J(\boldsymbol{f}).N+1}]\right)/std(E_{N+1})\right] \tag{7}$$

It can be observed that mapping (7) exhibits all properties listed at the beginning of this section. Figure 5 shows the exemplary $T(\boldsymbol{f})$ for two-dimensional objective space.

3.3. Nested Kriging with Variable-Thickness Domain

Incorporating the concept of variable-thickness domain into the nested kriging surrogate is straightforward. The domain definition (5) still holds, the only difference is the definition of extension coefficients (3) which now takes the form of

$$\boldsymbol{\alpha}(\boldsymbol{f}) = [\alpha_1(\boldsymbol{f}) \ldots \alpha_{n-N}(\boldsymbol{f})]^T = 0.5T(\boldsymbol{f})\left[|\boldsymbol{x}_d\boldsymbol{v}_n^{(1)}(\boldsymbol{f})| \ \ldots \ |\boldsymbol{x}_d\boldsymbol{v}_n^{(n-N)}(\boldsymbol{f})|\right]^T \tag{8}$$

with $T(\boldsymbol{f})$ given by (7).

A few comments should be made about the design of experiments procedure. In the original nested kriging with the fixed domain thickness parameter T, uniform sampling is straightforward

owing to a one-to-one mapping between the unit interval $[0,1]^n$ onto X_S. Given the point $\boldsymbol{z} \in [0,1]^n$, the mapping h_1 [51]

$$\begin{aligned} \boldsymbol{y} = h_1(\boldsymbol{z}) = h_1([z_1 \ \dots \ z_n]^T) = [f_{1.\min} + z_1(f_{1.\max} - f_{1.\min}) \ \cdots \\ \cdots \ f_{N.\min} + z_N(f_{N.\max} - f_{N.\min})] \times [-1 + 2z_{N+1} \ \dots \ -1 + 2z_n] \end{aligned} \tag{9}$$

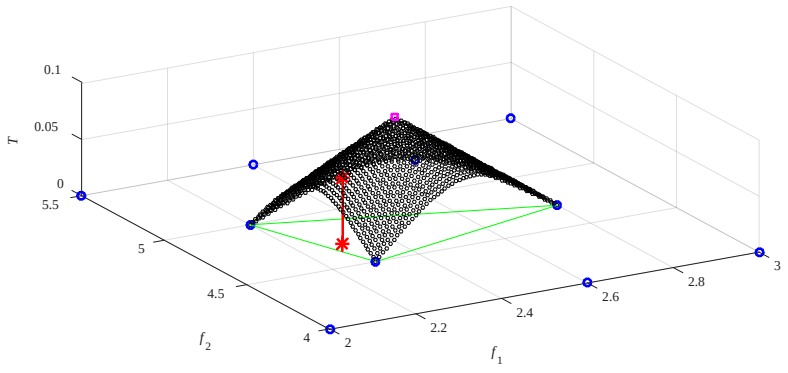
transforms $[0,1]^n$ onto the Cartesian product $F \times [-1,1]^{n-N}$. Subsequently, the function h_2

$$\begin{aligned} \boldsymbol{x} = h_2(\boldsymbol{y}) = h_2([y_1 \ \dots \ y_n]^T) = \boldsymbol{s}_I([y_1 \ \dots \ y_N]^T) + \\ + \sum_{k=1}^{n-N} y_{N+k}\alpha_k([y_1 \ \dots \ y_N]^T)\boldsymbol{v}_n^{(k)}([y_1 \ \dots \ y_N]^T) \end{aligned} \tag{10}$$

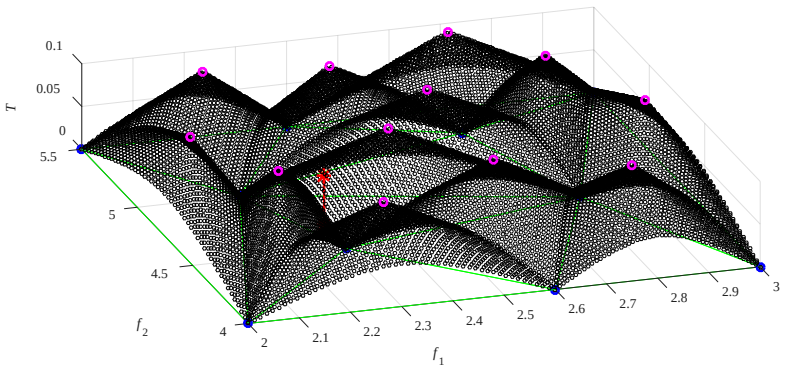
maps $F \times [-1,1]^{n-N}$ onto X_S. Using these, uniformly distributed samples $\boldsymbol{x}_B{}^{(k)}$ in X_S are obtained as

$$\boldsymbol{x}_B^{(k)} = H(\boldsymbol{z}^{(k)}) = h_2(h_1(\boldsymbol{z}^{(k)})) \tag{11}$$

where $\{\boldsymbol{z}^{(k)}\}$, $k = 1, \dots, N_B$, are uniformly distributed data points in $[0,1]^n$, here, obtained using Latin Hypercube Sampling [54].



(**a**)



(**b**)

Figure 5. Visualization of the thickness parameter function $T(\boldsymbol{f})$ for the exemplary objective space F: (**a**) a selected simplex and the corresponding thickness function. The vertical line illustrates the thickness value for a particular objective vector marked $*$; (**b**) $T(\boldsymbol{f})$ for the entire objective space. The reference objective vectors $\boldsymbol{f}^{(j)}$ are shown using circles on the f_1-f_2 plane; the local maxima of $T(\boldsymbol{f})$ correspond to the simplex centers $\boldsymbol{f}_T{}^{(j)}$.

In the case of variable-thickness domain, the situation is more complex. Although the mapping (11) can still be used, the obtained sample allocation will not be uniform (w.r.t. to the objective space) because the sample distribution will be compressed in the vicinity of the reference designs. This would not bring any computational advantages: when using the above strategy, the sample density remains the same as for the fixed-thickness case around the simplex centers $\boldsymbol{f}_T^{(j)}$ but will be unnecessarily high around the reference points $\boldsymbol{f}^{(j)}$. In this work, a different approach is employed. More specifically, the procedure (9)–(11) is used for $T = T_{\max}$, then all data samples $\boldsymbol{x}_B^{(k)}$ such that $\boldsymbol{x}_B^{(k)} \notin X_S$ are rejected and the EM antenna model is not evaluated therein. Additionally, the training data set is supplemented by all reference designs. This allows for maintaining uniform sample density throughout the domain and leads to significant computational savings as demonstrated in Section 4.

4. Numerical Results

This section presents the results of numerical validation of nested kriging modelling with variable-thickness domain. The method is compared to conventional surrogates (kriging and RBF) as well as the original nested kriging employing the fixed thickness parameter. The benchmark set includes two antenna structures, a dual-band dipole, and a broadband patch antenna with narrow ground plane.

4.1. Case I: Dual-Band Microstrip Dipole Antenna

Our first example is a dual-band dipole antenna shown in Figure 6 [55]. The structure is implemented on Rogers RO4003 substrate ($\varepsilon_r = 3.38$, $h = 0.76$ mm) and described by eight independent parameters: $\boldsymbol{x} = [L_{rr}\ d\ W_s\ W_d\ S\ L_d\ L_{gr}\ W_{gr}]^T$ (all dimensions in mm except those with r-subscript which are relative). The parameters $W_r = 5$, $L_s = 5$, and $L_0 = 25$ are fixed. The feed line width $W_0 = 4.5$ mm is calculated to ensure 50 ohm impedance. Other parameters are $L_r = L_{rr}((W_s - W_0)/2 - W_d - d)$, $W_g = W_{gr}W_s$, $L_g = L_{gr}(L_0 - W_g/2 + W_0/2)$, and $g = W_d$. The computational model is implemented in CST Microwave Studio (~900,000 mesh cells, simulation time 250 seconds).

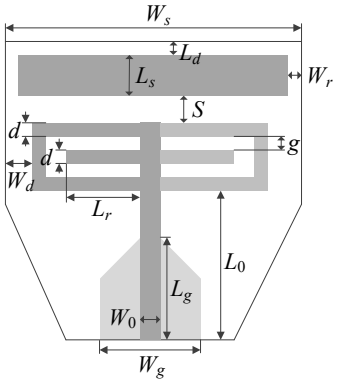
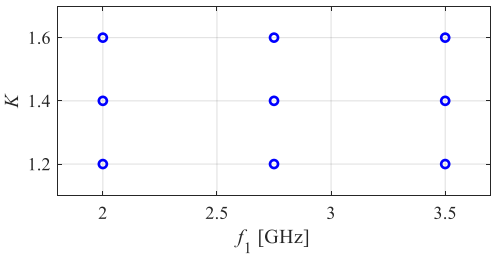


Figure 6. Dual-band dipole antenna geometry [55]. Ground plane shown using the light-gray shade.

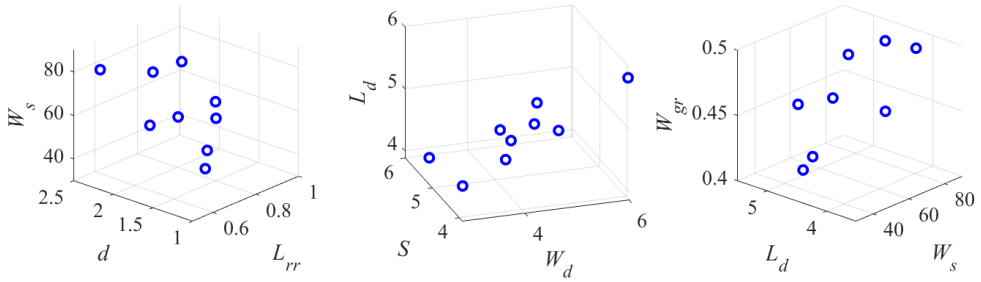
The surrogate model is to be constructed for the objective space parameterized by the operating frequencies f_1 and $f_2 = Kf_1$ for 2.0 GHz $\leq f_1 \leq$ 3.5 GHz, and $1.2 \leq K \leq 1.6$. Nine reference designs (for their allocation see Figure 7) are assigned, optimized for all combinations of $f_1 \in \{2.0, 2.75, 3.5\}$ GHz and $K \in \{1.2, 1.4, 1.6\}$. The parameter space X is determined by the lower and upper bounds for design variables, $\boldsymbol{l} = [0.55\ 1.0\ 47.0\ 2.5\ 3.8\ 3.8\ 0.5\ 0.24]^T$, and $\boldsymbol{u} = [1.0\ 2.5\ 77.0\ 6.5\ 6.0\ 6.0\ 1.0\ 0.5]^T$, set up using the reference points. For the sake of computational efficiency, the reference designs are obtained using the feature-based optimization framework [31].

Numerical verification of the proposed approach has been realized by constructing the surrogate model for several training data sets of various sizes as reported in Table 1. The nested kriging with variable-thickness domain has been compared to conventional surrogates (kriging and radial basis functions) as well as the (original) nested kriging with fixed domain thickness [51]. The nested kriging

models have been constructed for two values of T_{max}, 0.02 and 0.05. It can be observed that both nested kriging models (with the fixed-thickness and variable-thickness domains) exhibit comparable predictive power for the training data set sizes from 200 samples up (for original nested kriging model) and 50 samples for the proposed model, which is much better than that of the conventional surrogates. For smaller data sets, the results for the proposed model are not representative because of very limited numbers of samples (15 and 19, respectively), which makes the estimation of the predictive power unreliable. It should be emphasized that the number of training samples required by the variable-thickness models is significantly smaller. The computational savings are as high as 75 percent with the average of 70 percent over the considered training data sets. Figure 8 shows the surrogate responses for the variable-thickness nested kriging model at the selected testing designs along with the corresponding EM simulation data. The visual agreement between the characteristics is satisfactory.



(**a**)



(**b**)

Figure 7. Allocation of the reference designs for the dual-band antenna of Figure 6: (**a**) objective space, (**b**) selected three-dimensional projections of the parameter space.

Table 1. Modeling Results for Antenna of Figure 6.

Number of Training Samples	Relative RMS Error				Number of Training Samples *	Relative RMS Error	
	Conventional Models (Domain *X*)		(Original) Nested Kriging with Fixed Domain Thickness			Nested Kriging with Variable-Thickness Domain [this Work]	
	Kriging	RBF	T_{max} = 0.02	T_{max} = 0.05		T_{max} = 0.02	T_{max} = 0.05
50	55.6%	58.1%	14.5%	18.9%	15	25.7%	31.2%
100	46.7%	46.9%	11.2%	13.5%	19	18.3%	22.5%
200	41.9%	44.1%	6.9%	7.8%	55	8.9%	12.1%
400	36.9%	41.2%	6.1%	6.6%	108	5.9%	6.9%
800	35.5%	37.5%	4.1%	4.9%	208	5.0%	6.7%
1600	33.2%	35.8%	3.9%	4.2%	405	4.3%	3.8%

* The number of training samples is determined by the relative volume of the variable-thickness and fixed-thickness domains (see the design of experiments procedure description at the end of Section 3).

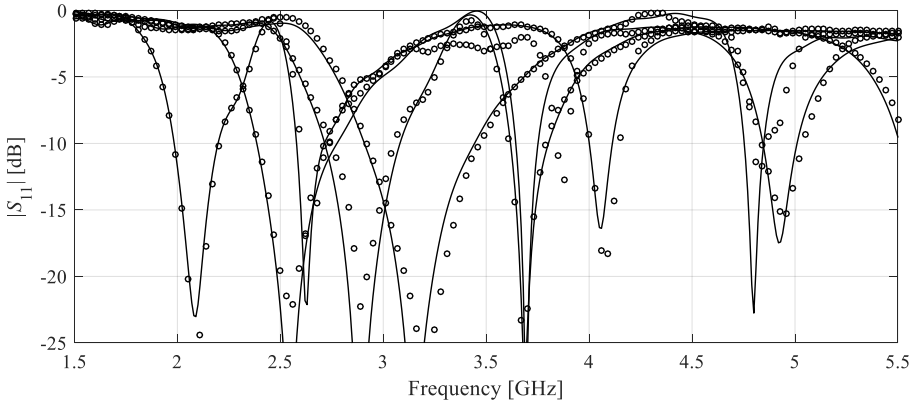


Figure 8. Dipole antenna: reflection responses at the selected test designs: EM model (—), nested kriging with variable-thickness domain obtained using 400 training samples and $T_{\max} = 0.02$ (o).

Supplementary validation has been conducted to determine whether variable-thickness domain affects the design utility of the surrogates. Figure 9 shows the initial and the optimized designs obtained for the selected objective vectors. It can be observed that the designs obtained by optimizing the fixed- and variable-thickness domain surrogates are comparable.

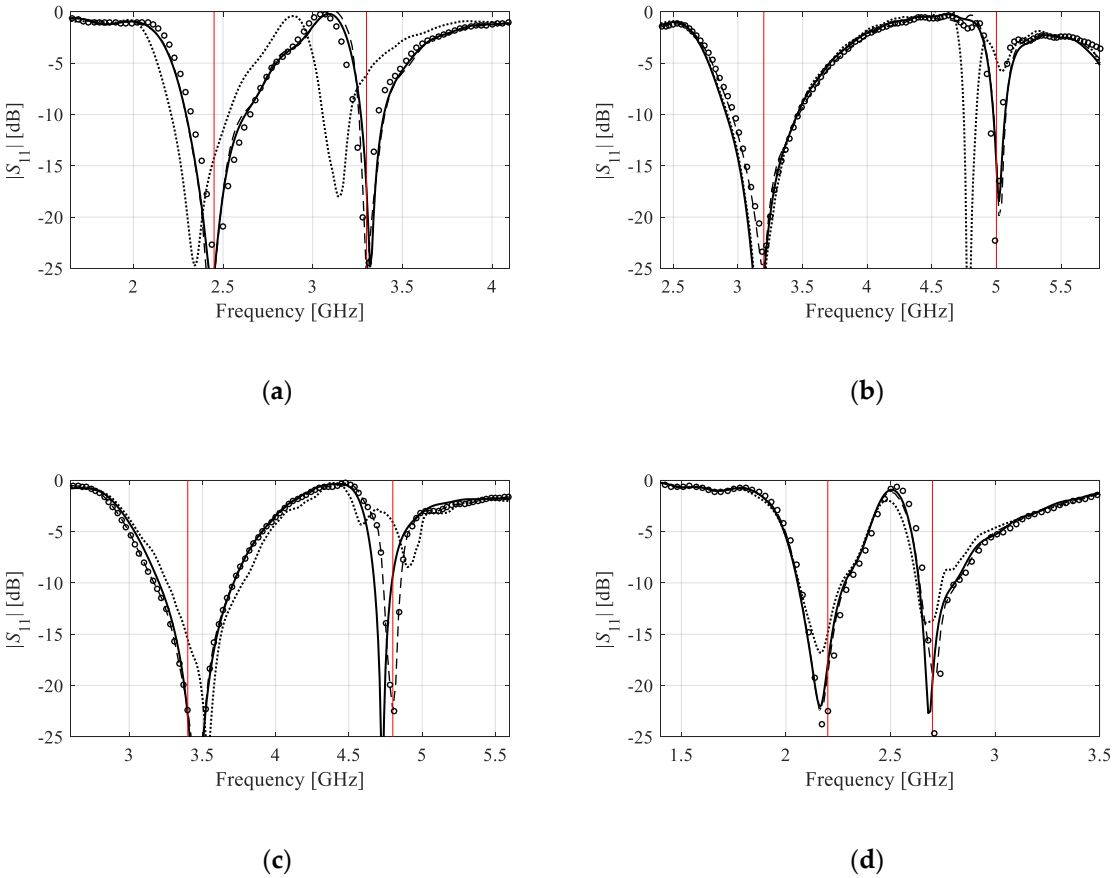
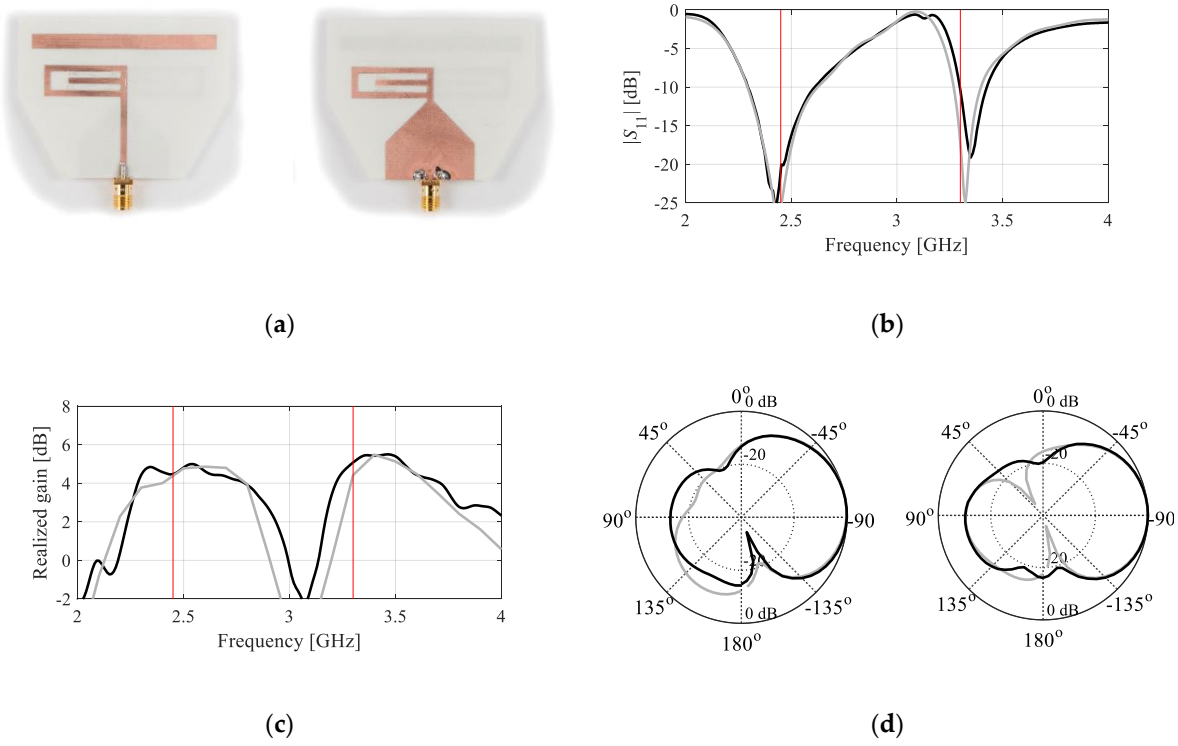


Figure 9. Optimization of the antenna of Figure 6 using the variable-thickness nested kriging surrogate for the four pairs of operating frequencies: (**a**) $f_1 = 2.45$ GHz, $f_2 = 3.3$ GHz, (**b**) $f_1 = 3.2$ GHz, $f_2 = 5.0$ GHz, (**c**) $f_1 = 3.4$ GHz, $f_2 = 4.8$ GHz, (**d**) $f_1 = 2.2$ GHz, $f_2 = 2.7$ GHz. Shown are: the initial design obtained from the first-level kriging model (····), response of the optimized variable-thickness nested kriging surrogate (- - -), response of the optimized fixed-thickness surrogate (o), and EM-simulated antenna response at the variable-thickness surrogate model optimum (—).

This indicates that restricting the domain does not compromise the model ability to yield high-quality designs. This was to be expected because the very definition of the variable-thickness domain is founded on reducing the thickness in the vicinity of the reference designs (where the image of the first-level model agrees perfectly with the optimum design manifold) and increasing it between the reference points (where the two manifolds deviate from each other).

The design optimized for f_1 = 2.45 GHz and f_2 = 3.3 GHz has been fabricated and measured for additional validation. Figure 10 shows the photographs of the antenna prototype, the reflection and realized gain characteristics, as well as the H- and E-plane radiation patterns. The agreement between the simulation and measurement data is satisfactory.



(**a**) (**b**) (**c**) (**d**)

Figure 10. Antenna of Figure 6 optimized for f_1 = 2.45 GHz, f_2 = 3.3 GHz: (**a**) photographs of the prototype, (**b**) reflection $|S_{11}|$, (**c**) end-fire realized gain, (**d**) yz-plane radiation pattern at both operating frequencies (2.45 GHz and 3.3 GHz on the left- and right-hand-side, respectively). Simulated and measured characteristics shown in gray and black, respectively.

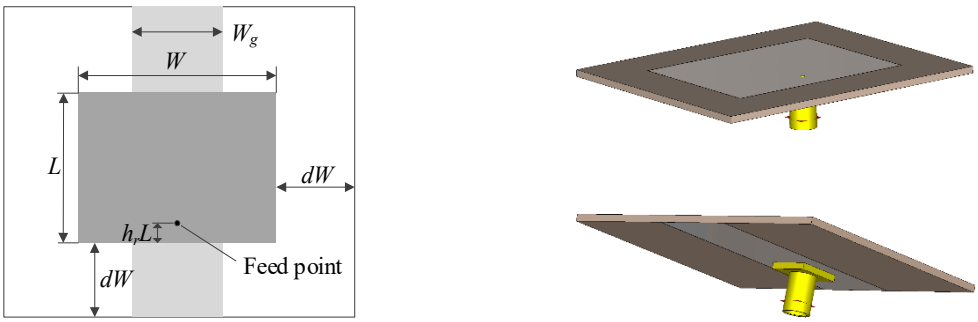
4.2. Case II: Broadband Patch Antenna

The second example is a broadband patch antenna with a narrow ground plane shown in Figure 11 [56]. The structure is described by five parameters $\boldsymbol{x} = [W\ L\ dW\ W_g\ h_r]^T$. The computational model is implemented in CST Microwave Studio and evaluated using the transient solver (~400,000 cells, simulation time 94 seconds).

The substrate parameters, dielectric permittivity ε_r and height h are the operating conditions being a part of the objective space. The model incorporates the SMA connector. The design optimality is understood as minimization of the antenna reflection within at least 10-percent fractional bandwidth symmetric w.r.t. the target center frequency f_0.

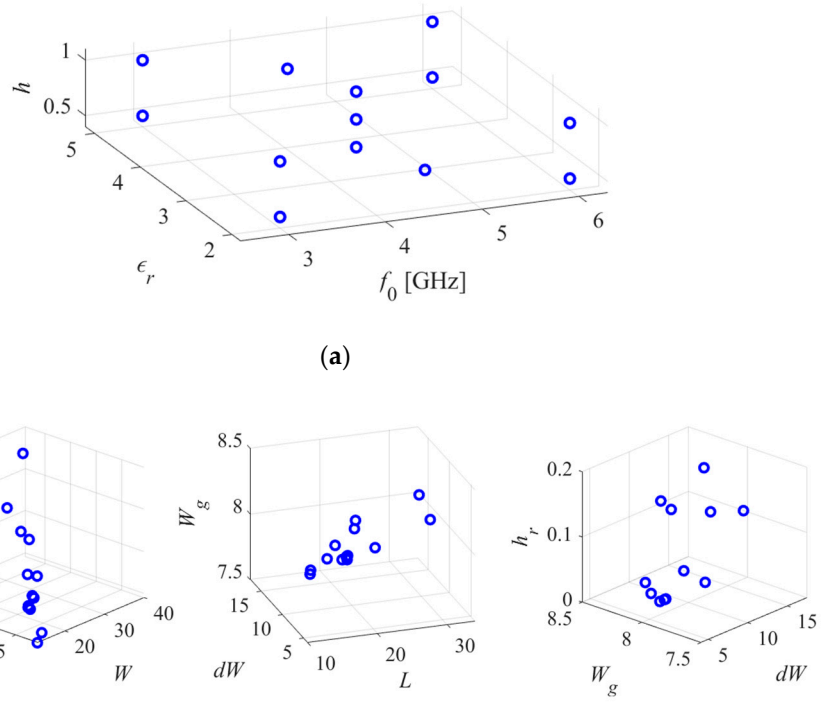
We aim at constructing the surrogate model within the objective space defined by the following ranges of the center frequency and surrogate parameters: 3.0 GHz $\leq f_0 \leq$ 6.0 GHz, permittivity 2.0 $\leq \varepsilon_r \leq$ 5.0 and height 0.5 mm $\leq h \leq$ 1.0 mm. There are thirteen reference designs assigned (shown in Figure 12), corresponding to $\{f_0,\varepsilon_r,h\}$ = {3.0,2.0,0.5}, {3.0,2.0,1.0}, {3.0,5.0,0.5}, {3.0,5.0,1.0}, {4.5,3.5,0.75}, {4.5,3.5,0.5}, {4.5,3.5,1.0}, {4.5,2.0,0.75}, {4.5,5.0,0.75}, {6.0,2.0,0.5}, {6.0,2.0,1.0}, {6.0,5.0,0.5}, and {6.0,5.0,1.0}.

The parameter space X is determined by the lower and upper bounds for design variables $\boldsymbol{l} = [12.5\ 10.0\ 4.0\ 8.0\ 0.02]^T$, and $\boldsymbol{u} = [40.0\ 34.0\ 17.0\ 10.0\ 0.2]^T$.



(**a**) (**b**)

Figure 11. Broadband patch antenna [56]: (**a**) geometry (ground plane shown using light gray shade), (**b**) 3D views.



(**a**)

(**b**)

Figure 12. Allocation of the reference designs for the antenna of Figure 11: (**a**) objective space, (**b**) selected three-dimensional projections of the parameter space.

Model validation has been arranged similarly as for the first example. Table 2 shows the numerical data for the models constructed using the training data sets of different sizes. The benchmark methods include conventional models established in the parameter space X (kriging interpolation and radial basis functions), as well as the nested kriging with fixed-thickness domain. The nested kriging models have been constructed for the two values of $T_{\max}$, 0.025 and 0.05. The obtained results are consistent with those reported in Section 4.1. In particular, the accuracy of both nested kriging models (with the fixed-thickness and variable-thickness domains) is essentially the same; however, the number of samples required by the variable-thickness domain model is considerably smaller.

Table 2. Modeling Results for Antenna of Figure 11.

Number of Training Samples	Relative RMS Error				Number of Training Samples *	Relative RMS Error	
	Conventional Models (Domain *X*)		(Original) Nested Kriging with Fixed Domain Thickness			Nested Kriging with Variable-Thickness Domain [this Work]	
	Kriging	RBF	T_{max} = 0.025	T_{max} = 0.05		T_{max} = 0.025	T_{max} = 0.05
50	43.4%	52.0%	10.1%	17.8%	30	13.0%	14.8%
100	21.2%	25.4%	7.9%	9.0%	63	7.8%	9.1%
200	16.0%	18.2%	7.2%	6.5%	125	7.3%	6.4%
400	12.8%	14.7%	4.7%	6.1%	247	4.9%	5.3%
800	9.8%	11.3%	3.3%	4.8%	505	3.8%	5.1%

* The number of training samples is determined by the relative volume of the variable-thickness and fixed-thickness domains (see the design of experiments procedure description at the end of Section 3).

The computational savings are close to forty percent. The responses for the variable-thickness nested kriging model at the selected testing designs along with the corresponding EM simulation data are shown in Figure 13.

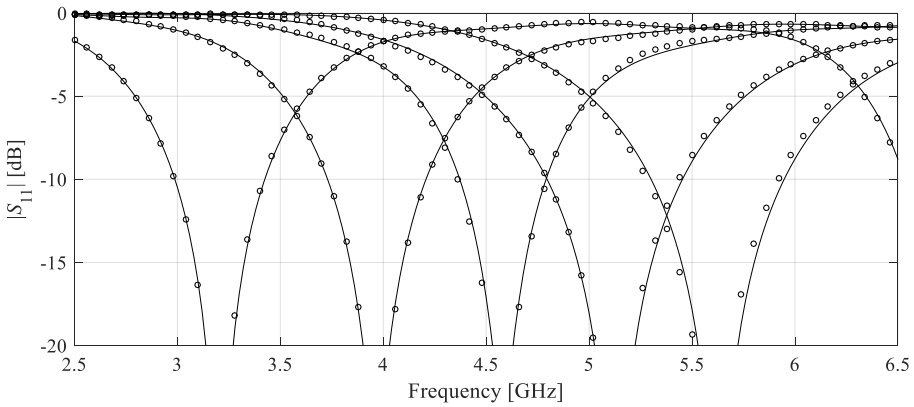


Figure 13. Patch antenna: reflection responses at the selected test designs: EM model (—), nested kriging with variable-thickness domain obtained using 800 training samples and T_{max} = 0.05 (o).

The proposed surrogate has been employed for antenna optimization to provide an additional validation. The objective was to assess whether variable-thickness domain affects the model capability to reach the optimum design across the objective space. The results obtained for selected objective vectors have been shown in Figure 14. It can be noted that the designs produced by variable- and fixed-thickness domain models are of comparable quality, which corroborates the design utility of the presented technique.

One of the optimized designs, corresponding to f_0 = 4.8 GHz, ε_r = 3.38, h = 0.51 mm, has been fabricated and measured for additional validation. The antenna structure has been implemented on Rogers RO4003C substrate. Figure 15 shows the photographs of the antenna prototype, the reflection and realized gain characteristics, as well as the H- and E-plane radiation patterns. The agreement between the simulation and measurement data is satisfactory.

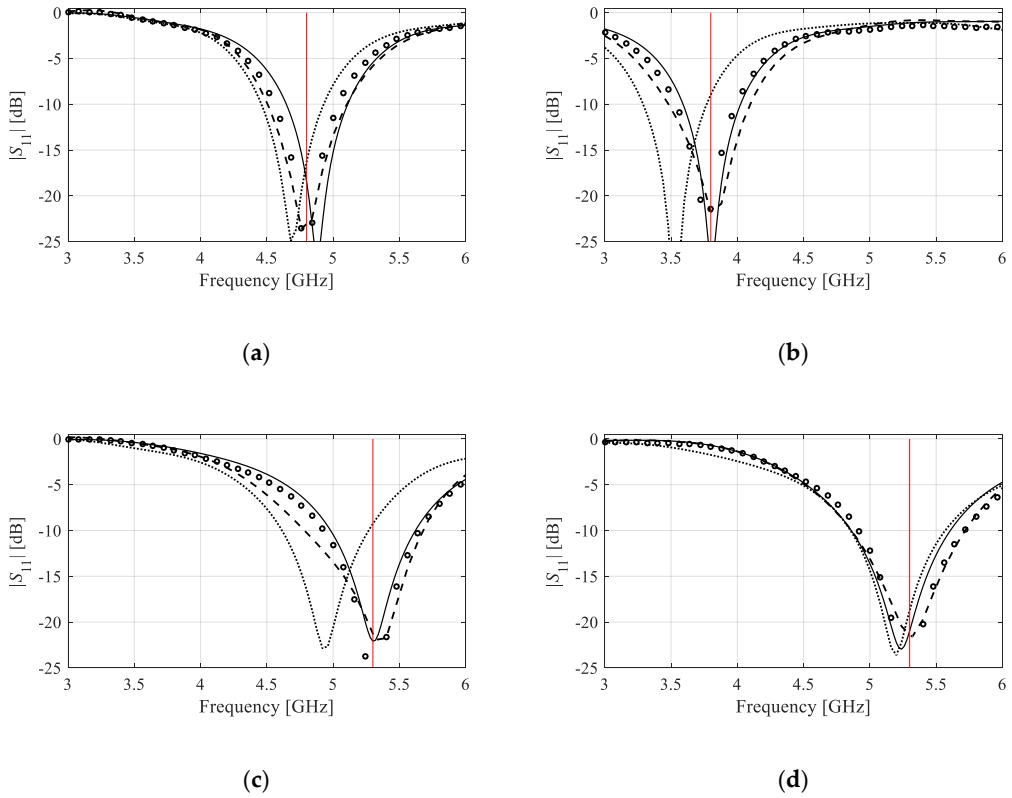


Figure 14. Optimization of the antenna of Figure 11 using the variable-thickness nested kriging surrogate set up using 800 samples ($T_{\max} = 0.05$): initial design obtained from the first-level model (····), surrogate model response at the optimized design obtained using variable thickness model (- - -), response of the optimized fixed-thickness surrogate (o), EM simulated response at the variable-thickness surrogate model optimum (—): (**a**) $f_0 = 4.8$ GHz, $\varepsilon_r = 3.38$, $h = 0.51$ mm, (**b**) $f_0 = 3.8$ GHz, $\varepsilon_r = 2.5$, $h = 0.76$ mm, (**c**) $f_0 = 5.3$ GHz, $\varepsilon_r = 3.38$, $h = 0.81$ mm, (**d**) $f_0 = 5.3$ GHz, $\varepsilon_r = 4.4$, $h = 1.0$ mm.

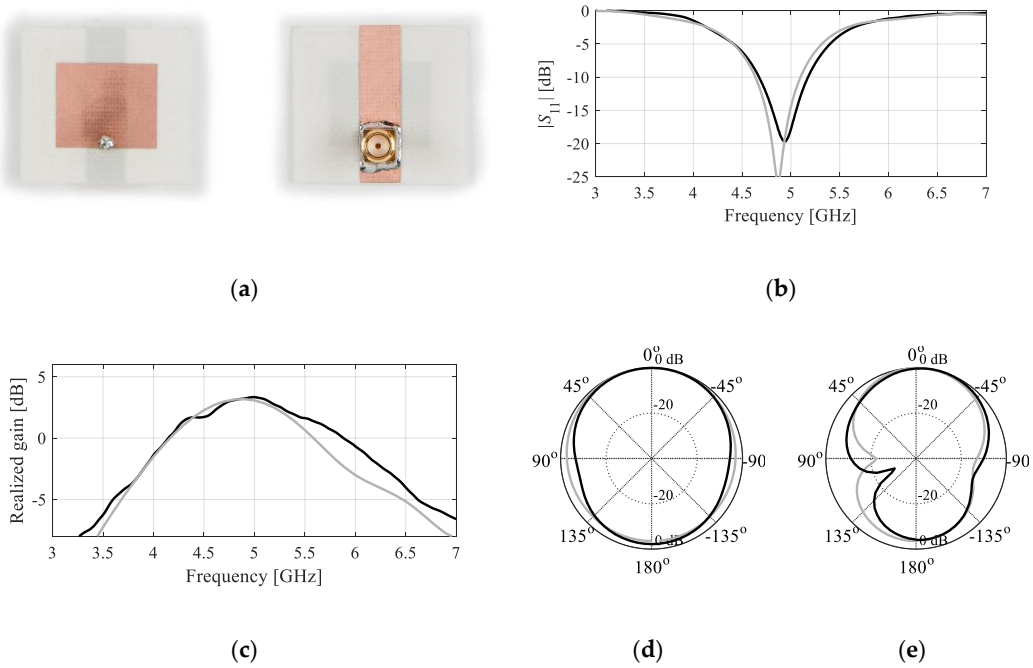


Figure 15. Antenna of Figure 11 optimized for $f_0 = 4.8$ GHz, $\varepsilon_r = 3.38$ and $h = 0.51$ mm, implemented on RO4003C substrate: (**a**) antenna prototype, (**b**) reflection, (**c**) realized gain, (**d**) H-plane pattern at 4.8 GHz, (**e**) E-plane pattern at 4.8 GHz; simulations (gray) and measurements (black).

5. Conclusions

The paper proposed a novel variation of the nested kriging framework, the recent performance-driven modelling method. The keystone of our approach was to introduce a functional dependence of the lateral size (thickness) of the surrogate model domain on the objective space location. This approach was motivated by the fact that the first-level model uncertainty (in terms of representing the optimum design manifold) ranges from zero at the reference designs used to set up the surrogate, to its maxima between these designs. From this perspective, maintaining fixed domain thickness, as in the original nested kriging, is not imperative.

The variable-thickness domain developed in this work enables a significant reduction of the training data set size without compromising the model accuracy. The presented concept has been explained, formalized, and its implementation has been validated in a comprehensive manner using two examples of microstrip antennas. The numerical results conclusively demonstrate that the computational savings pertinent to training data acquisition can be as high as seventy percent while maintaining the predictive power of the surrogates essentially intact as compared to the fixed-thickness version. The same has been observed concerning the design utility of the models, i.e., their ability to encapsulate the optimum designs across the entire objective space.

The authors believe that the presented methodology is a step towards the development of computationally efficient methodologies for reliable modelling of antenna structures. Perhaps the most important aspect is addressing the dimensionality and parameter range issues that normally constitute the most serious obstacle for constructing accurate and representations for antenna systems. Appropriate combination of various approaches, here, the nested kriging model, and variable-thickness domain, allow for further enhancement of already efficient procedure, and construction of metamodels using very small number of training data samples. The error levels achieved for the presented verification examples are—given a small number of EM data samples required to render the surrogates—way beyond what has been offered in the literature so far. The future work will be focused on generalization of the technique to enable efficient modelling in higher-dimensional parameter spaces.

Author Contributions: Conceptualization, S.K. and A.P.-D.; methodology, S.K. and A.P.-D.; software, S.K. and A.P.-D.; validation, S.K. and A.P.-D.; formal analysis, S.K.; investigation, S.K. and A.P.-D.; resources, S.K.; data curation, S.K. and A.P.-D.; writing—original draft preparation, S.K. and A.P.-D.; writing—review and editing, S.K. and A.P.-D.; visualization, S.K. and A.P.-D.; supervision, S.K.; project administration, S.K.; funding acquisition, S.K. All authors have read and agreed to the published version of the manuscript.

Funding: This work was supported in part by the Icelandic Centre for Research (RANNIS) Grant 206606051, and by National Science Centre of Poland Grant 2017/27/B/ST7/00563.

Acknowledgments: The authors thank Dassault Systemes, France, for making CST Microwave Studio available.

Conflicts of Interest: The authors declare no conflict of interest. The funders had no role in the design of the study; in the collection, analyses, or interpretation of data; in the writing of the manuscript, or in the decision to publish the results.

References

1. Guo, D.; He, K.; Zhang, Y.; Song, M. A Multiband Dual-Polarized Omnidirectional Antenna for Indoor Wireless Communication Systems. *IEEE Antennas Wirel. Propag. Lett.* **2016**, *16*, 290–293. [CrossRef]
2. Zeng, J.; Luk, K.M. Single-Layered Broadband Magnetoelectric Dipole Antenna for New 5G Application. *IEEE Antennas Wirel. Propag. Lett.* **2019**, *18*, 911–915. [CrossRef]
3. Nie, Z.; Zhai, H.; Liu, L.; Li, J.; Hu, D.; Shi, J. A Dual-Polarized Frequency-Reconfigurable Low-Profile Antenna with Harmonic Suppression for 5G Application. *IEEE Antennas Wirel. Propag. Lett.* **2019**, *18*, 1228–1232. [CrossRef]
4. Mener, S.; Gillard, R.; Roy, L. A Dual-Band Dual-Circular-Polarization Antenna for Ka-Band Satellite Communications. *IEEE Antennas Wirel. Propag. Lett.* **2017**, *16*, 274–277. [CrossRef]

5. Felício, J.M.; Bioucas-Dias, J.M.; Costa, J.R.; Fernandes, C.A. Antenna Design and Near-Field Characterization for Medical Microwave Imaging Applications. *IEEE Trans. Antennas Propag.* **2019**, *67*, 4811–4824. [CrossRef]
6. Jha, K.R.; Bukhari, B.; Singh, C.; Mishra, G.; Sharma, S.K. Compact Planar Multistandard MIMO Antenna for IoT Applications. *IEEE Trans. Antennas Propag.* **2018**, *66*, 3327–3336. [CrossRef]
7. Qian, J.-F.; Chen, F.-C.; Xiang, K.-R.; Chu, Q.-X. Resonator-Loaded Multi-Band Microstrip Slot Antennas with Bidirectional Radiation Patterns. *IEEE Trans. Antennas Propag.* **2019**, *67*, 6661–6666. [CrossRef]
8. Ullah, U.; Koziel, S. A Broadband Circularly Polarized Wide-Slot Antenna with a Miniaturized Footprint. *IEEE Antennas Wirel. Propag. Lett.* **2018**, *17*, 2454–2458. [CrossRef]
9. Xu, Y.; Wang, J.; Ge, L.; Wang, X.; Wu, W. Design of a Notched-Band Vivaldi Antenna with High Selectivity. *IEEE Antennas Wirel. Propag. Lett.* **2018**, *17*, 62–65. [CrossRef]
10. Zhao, A.; Ren, Z. Size Reduction of Self-Isolated MIMO Antenna System for 5G Mobile Phone Applications. *IEEE Antennas Wirel. Propag. Lett.* **2018**, *18*, 152–156. [CrossRef]
11. Dong, Y.; Choi, J.; Itoh, T. Vivaldi Antenna with Pattern Diversity for 0.7 to 2.7 GHz Cellular Band Applications. *IEEE Antennas Wirel. Propag. Lett.* **2018**, *17*, 247–250. [CrossRef]
12. Yan, S.; Soh, P.J.; VandenBosch, G.A.E. Wearable Dual-Band Magneto-Electric Dipole Antenna for WBAN/WLAN Applications. *IEEE Trans. Antennas Propag.* **2015**, *63*, 1. [CrossRef]
13. Wang, J.; Leach, M.; Lim, E.G.; Wang, Z.; Pei, R.; Huang, Y. An Implantable and Conformal Antenna for Wireless Capsule Endoscopy. *IEEE Antennas Wirel. Propag. Lett.* **2018**, *17*, 1153–1157. [CrossRef]
14. Fakih, M.A.; Diallo, A.; Le Thuc, P.; Staraj, R.; Mourad, O.; Rachid, E.A. Optimization of Efficient Dual Band PIFA System for MIMO Half-Duplex 4G/LTE and Full-Duplex 5G Communications. *IEEE Access* **2019**, *7*, 128881–128895. [CrossRef]
15. Hassan, E.; Noreland, D.; Augustine, R.; Wadbro, E.; Berggren, M. Topology Optimization of Planar Antennas for Wideband Near-Field Coupling. *IEEE Trans. Antennas Propag.* **2015**, *63*, 4208–4213. [CrossRef]
16. Tsukamoto, K.; Arai, H. Optimization of smooth walled horn antenna using multilevel fast multipole method. In Proceedings of the 2016 International Symposium on Antennas and Propagation (ISAP), Okinawa, Japan, 24–28 October 2016.
17. Lalbakhsh, A.; Afzal, M.U.; Esselle, K.P. Multi-objective Particle Swarm Optimization to Design a Time Delay Equalizer Metasurface for an Electromagnetic Band Gap Resonator Antenna. *IEEE Antennas Wirel. Propag. Lett.* **2016**, *16*, 1. [CrossRef]
18. Wang, J.; Yang, X.S.; Wang, B.Z. Efficient gradient-based optimization of pixel antenna with large-scale connections. *IET Microw. Ant. Prop.* **2018**, *12*, 385–389. [CrossRef]
19. Koziel, S.; Ogurtsov, S.; Cheng, Q.S.; Bandler, J.W. Rapid EM-based microwave design optimization exploiting shape-preserving response prediction and adjoint sensitivities. *IET Microw. Ant. Prop.* **2014**, *8*, 775–781. [CrossRef]
20. Koziel, S.; Pietrenko-Dabrowska, A. Reduced-cost electromagnetic-driven optimization of antenna structures by means of trust-region gradient-search with sparse Jacobian updates. *IET Microw. Ant. Prop.* **2019**, *13*, 1646–1652. [CrossRef]
21. Koziel, S.; Pietrenko-Dabrowska, A. Variable-Fidelity Simulation Models and Sparse Gradient Updates for Cost-Efficient Optimization of Compact Antenna Input Characteristics. *Sensors* **2019**, *19*, 1806. [CrossRef]
22. Easum, J.A.; Nagar, J.; Werner, P.L.; Werner, D.H. Efficient Multiobjective Antenna Optimization with Tolerance Analysis Through the Use of Surrogate Models. *IEEE Trans. Antennas Propag.* **2018**, *66*, 6706–6715. [CrossRef]
23. Hassan, A.-K.S.; Etman, A.S.; Soliman, E.A. Optimization of a Novel Nano Antenna with Two Radiation Modes Using Kriging Surrogate Models. *IEEE Photon- J.* **2018**, *10*, 1–17. [CrossRef]
24. Easum, J.A.; Nagar, J.; Werner, D.H. Multi-objective surrogate-assisted optimization applied to patch antenna design. In Proceedings of the 2017 IEEE International Symposium on Antennas and Propagation, San Diego, CA, USA, 9–14 July 2017; pp. 339–340.
25. De Villiers, D.I.; Couckuyt, I.; Dhaene, T. Multi-objective optimization of reflector antennas using kriging and probability of improvement. In Proceedings of the 2017 IEEE International Symposium on Antennas and Propagation, San Diego, CA, USA, 9–14 July 2017; pp. 985–986.
26. Dong, J.; Qin, W.; Wang, M. Fast Multi-Objective Optimization of Multi-Parameter Antenna Structures Based on Improved BPNN Surrogate Model. *IEEE Access* **2019**, *7*, 77692–77701. [CrossRef]

27. Du, J.; Roblin, C. Stochastic surrogate models of deformable antennas based on vector spherical harmonics and polynomial chaos expensions: Application to textile antennas. *IEEE Trans. Ant. Prop.* **2018**, *66*, 3610–3622. [CrossRef]
28. Rayas-Sanchez, J.E. Power in Simplicity with ASM: Tracing the Aggressive Space Mapping Algorithm Over Two Decades of Development and Engineering Applications. *IEEE Microw. Mag.* **2016**, *17*, 64–76. [CrossRef]
29. Cervantes-González, J.C.; Rayas-Sánchez, J.E.; López, C.A.; Camacho-Pérez, J.R.; Brito, Z.B.; Chavez-Hurtado, J.L. Space mapping optimization of handset antennas considering EM effects of mobile phone components and human body. *Int. J. RF Microw. Comput. Eng.* **2015**, *26*, 121–128. [CrossRef]
30. Koziel, S.; Unnsteinsson, S.D. Expedited Design Closure of Antennas by Means of Trust-Region-Based Adaptive Response Scaling. *IEEE Antennas Wirel. Propag. Lett.* **2018**, *17*, 1099–1103. [CrossRef]
31. Koziel, S. Fast simulation-driven antenna design using response-feature surrogates. *Int. J. RF Microw. Comput. Eng.* **2014**, *25*, 394–402. [CrossRef]
32. Koziel, S.; Ogurtsov, S. *Antenna Design by Simulation-Driven Optimization. Surrogate-Based Approach*; Springer: Berlin/Heidelberg, Germany, 2014.
33. Alzahed, A.M.; Mikki, S.; Antar, Y.M.M. Nonlinear Mutual Coupling Compensation Operator Design Using a Novel Electromagnetic Machine Learning Paradigm. *IEEE Antennas Wirel. Propag. Lett.* **2019**, *18*, 861–865. [CrossRef]
34. Tak, J.; Kantemur, A.; Sharma, Y.; Xin, H. A 3-D-Printed W-Band Slotted Waveguide Array Antenna Optimized Using Machine Learning. *IEEE Antennas Wirel. Propag. Lett.* **2018**, *17*, 2008–2012. [CrossRef]
35. Torun, H.M.; Swaminathan, M. High-Dimensional Global Optimization Method for High-Frequency Electronic Design. *IEEE Trans. Microw. Theory Tech.* **2019**, *67*, 2128–2142. [CrossRef]
36. Queipo, N.V.; Haftka, R.T.; Shyy, W.; Goel, T.; Vaidyanathan, R.; Tucker, P.K. Surrogate-based analysis and optimization. *Prog. Aerosp. Sci.* **2005**, *41*, 1–28. [CrossRef]
37. Barmuta, P.; Ferranti, F.; Gibiino, G.P.; Lewandowski, A.; Schreurs, D.M.M.-P. Compact Behavioral Models of Nonlinear Active Devices Using Response Surface Methodology. *IEEE Trans. Microw. Theory Tech.* **2014**, *63*, 56–64. [CrossRef]
38. Jacobs, J.P. Characterization by Gaussian processes of finite substrate size effects on gain patterns of microstrip antennas. *IET Microw. Ant. Prop.* **2016**, *10*, 1189–1195. [CrossRef]
39. Petrocchi, A.; Kaintura, A.; Avolio, G.; Spina, D.; Dhaene, T.; Raffo, A.; Schreurs, D.M.M.-P. Measurement Uncertainty Propagation in Transistor Model Parameters via Polynomial Chaos Expansion. *IEEE Microw. Wirel. Components Lett.* **2017**, *27*, 572–574. [CrossRef]
40. Gorissen, D.; Crombecq, K.; Couckuyt, I.; Dhaene, T.; Demeester, P. A surrogate modeling and adaptive sampling toolbox for computer based design. *J. Mach. Learn. Res.* **2010**, *11*, 2051–2055.
41. Marelli, S.; Sudret, B. UQLab: A Framework for Uncertainty Quantification in Matlab. In Proceedings of the 2nd International Conference on Vulnerability, Risk Analysis and Management, Liverpool, UK, 13–16 July 2014.
42. Rawat, A.; Yadav, R.; Shrivastava, S.C. Neural network applications in smart antenna arrays: A review. *AEU Int. J. Electron. Commun.* **2012**, *66*, 903–912. [CrossRef]
43. Cai, J.; King, J.; Yu, C.; Liu, J.; Sun, L. Support Vector Regression-Based Behavioral Modeling Technique for RF Power Transistors. *IEEE Microw. Wirel. Compon. Lett.* **2018**, *28*, 428–430. [CrossRef]
44. Yucel, A.C.; Bagci, H.; Michielssen, E. An ME-PC Enhanced HDMR Method for Efficient Statistical Analysis of Multiconductor Transmission Line Networks. *IEEE Trans. Compon. Packag. Manuf. Technol.* **2015**, *5*, 685–696. [CrossRef]
45. Hu, R.; Monebhurrun, V.; Himeno, R.; Yokota, H.; Costen, F. An Adaptive Least Angle Regression Method for Uncertainty Quantification in FDTD Computation. *IEEE Trans. Antennas Propag.* **2018**, *66*, 7188–7197. [CrossRef]
46. Jacobs, J.P.; Koziel, S. Two-Stage Framework for Efficient Gaussian Process Modeling of Antenna Input Characteristics. *IEEE Trans. Antennas Propag.* **2013**, *62*, 706–713. [CrossRef]
47. Kennedy, M. Predicting the output from a complex computer code when fast approximations are available. *Biometrika* **2000**, *87*, 1–13. [CrossRef]
48. Wang, F.; Cachecho, P.; Zhang, W.; Sun, S.; Li, X.; Kanj, R.; Gu, C. Bayesian Model Fusion: Large-Scale Performance Modeling of Analog and Mixed-Signal Circuits by Reusing Early-Stage Data. *IEEE Trans. Comput. Des. Integr. Circuits Syst.* **2015**, *35*, 1255–1268. [CrossRef]

49. Koziel, S. Low-Cost Data-Driven Surrogate Modeling of Antenna Structures by Constrained Sampling. *IEEE Antennas Wirel. Propag. Lett.* **2016**, *16*, 461–464. [CrossRef]
50. Koziel, S.; Sigurdsson, A.T. Triangulation-Based Constrained Surrogate Modeling of Antennas. *IEEE Trans. Antennas Propag.* **2018**, *66*, 4170–4179. [CrossRef]
51. Koziel, S.; Pietrenko-Dabrowska, A. Performance-Based Nested Surrogate Modeling of Antenna Input Characteristics. *IEEE Trans. Antennas Propag.* **2019**, *67*, 2904–2912. [CrossRef]
52. Forrester, A.I.; Keane, A. Recent advances in surrogate-based optimization. *Prog. Aerosp. Sci.* **2009**, *45*, 50–79. [CrossRef]
53. Borouchaki, H.; George, P.L.; Lo, S.H. Optimal Delaunay point insertion. *Int. J. Numer. Methods Eng.* **1996**, *39*, 3407–3437. [CrossRef]
54. Beachkofski, B.; Grandhi, R. *Improved Distributed Hypercube Sampling*; paper AIAA 2002-1274; American Institute of Aeronautics and Astronautics (AIAA): Reston, VA, USA, 2002.
55. Qudrat-E-Maula, M.; Shafai, L. A dual band microstrip dipole antenna. In Proceedings of the 2014 16th International Symposium on Antenna Technology and Applied Electromagnetics (ANTEM), Victoria, BC, Canada, 13–16 July 2014.
56. Wang, Y.; Lu, Y.; Lu, G.; Cao, W.; Kishk, A.A. Broadband Patch Antenna with Narrow Width Ground Plane. In Proceedings of the 2018 IEEE International Symposium on Antennas and Propagation, Boston, MA, USA, 8–13 July 2018.



© 2020 by the authors. Licensee MDPI, Basel, Switzerland. This article is an open access article distributed under the terms and conditions of the Creative Commons Attribution (CC BY) license (http://creativecommons.org/licenses/by/4.0/).